Nanoparticle generation and transport resulting from femtosecond laser ablation of ultrathin metal films: Time-resolved measurements and molecular dynamics simulations

C. M. Rouleau,[1,a)] C.-Y. Shih,[2] C. Wu,[2] L. V. Zhigilei,[2] A. A. Puretzky,[1] and D. B. Geohegan[1]
[1]*Center for Nanophase Materials Sciences, Oak Ridge National Laboratory, Oak Ridge, Tennessee 37831, USA*
[2]*Department of Materials Science and Engineering, University of Virginia, Charlottesville, Virginia 22904, USA*

(Received 2 April 2014; accepted 21 April 2014; published online 14 May 2014)

The synthesis of metal nanoparticles by ultrafast laser ablation of nanometers-thick metal films has been studied experimentally and computationally. Near-threshold backside laser ablation of 2–20 nm-thick Pt films deposited on fused silica substrates was found to produce nanoparticles with size distributions that were bimodal for the thicker films, but collapsed into a single mode distribution for the thinnest film. Time-resolved imaging of blackbody emission from the Pt nanoparticles was used to reveal the nanoparticle propagation dynamics and estimate their temperatures. The observed nanoparticle plume was compact and highly forward-directed with a well-defined collective velocity that permitted multiple rebounds with substrates to be revealed. Large-scale molecular dynamics simulations were used to understand the evolution of compressive and tensile stresses in the thicker melted liquid films that lead to their breakup and ejection of two groups of nanoparticles with different velocity and size distributions. Ultrafast laser irradiation of ultrathin (few nm) metal films avoids the splitting of the film and appears to be a method well-suited to cleanly synthesize and deposit nanoparticles from semitransparent thin film targets in highly directed beams. © *2014 AIP Publishing LLC*. [http://dx.doi.org/10.1063/1.4876601]

Controlling the synthesis and processing of novel metal and alloy nanoparticles is crucial for the fields of nanoelectronics, sensing, catalysis, and medical therapies.[1] When compared to chemical methods, laser ablation of solids offers a clean, surfactant-free, non-equilibrium processing approach to explore the synthesis of new nanoparticles with unique nanophases.[2,3] Ultrafast laser sources appear particularly well-suited for this purpose since a large fraction of the material ejected during ablation of solids has been shown to be nanoparticles.[4–9] In most cases, however, there still remains an ion plasma component[10] to the laser ablation plume that, through gas-phase or surface condensation, would also generate nanoparticles. Although the plasma component can be nearly eliminated by employing a laser fluence near threshold, there is unfortunately a commensurate and *rapid* reduction in the volume of material available for nanoparticle formation.[10] However, Murphy *et al.*[11] recently showed that a thin Ni film on a transparent substrate had a removal threshold nearly half that of bulk Ni, and this suggests that one can choose an ablation regime that eliminates the ion plasma component while still maintaining the ability to remove a significant amount of material for nanoparticle production.

We recently tested this using through thin film ablation (TTFA)[12] with a femtosecond laser source, and found that much like TTFA using a ns laser source, two populations of nanoparticles were produced in the deposit.[13] However, unlike ns-TTFA wherein elevated background gas pressures were observed to affect the nanoparticle populations by gas-phase condensation of atomic and molecular species within the plume, it was found that employing the same pressures as those used in Ref. 12 had *no* effect on the populations produced by fs-TTFA.

To understand this discrepancy and the mechanism of fs-TTFA, here we explore nanoparticle formation, transport dynamics, and size distributions as a function of metal film thickness for a laser fluence near the threshold for film removal.

Single 800 nm, 40 fs pulses from a Coherent Legend HE laser were attenuated and used to illuminate a rectangular aperture that was imaged through a 1.5 mm thick window onto the interface between 1 mm thick fused silica substrates and e-beam deposited Pt films. The laser spot size and incident fluence at the interface were 20 μm × 25 μm and 40–60 mJ/cm^2, respectively (see Ref. 13 for additional details). Films less than 20 nm thick were chosen in accordance with the ~13 nm optical penetration depth of Pt, to provide both complete and partial absorption conditions. A gated, intensified CCD (ICCD) camera was used to capture time-resolved, side-view images of the ejecta and its transport between source and receiving substrates. The entire processing chamber was mounted on an XYZ stage to provide a fresh Pt film region for every laser shot.

Fig. 1(c) shows a typical sequence of ICCD images obtained during backside ablation of a 20 nm Pt film in vacuum. Most notable in the figure was the formation of an unusual and compact, highly forward-directed plume that, contrary to those observed from bulk targets, had a high minimum velocity (~100 m/s for the trailing edge). The elongation of the plume in the propagation direction is similar to that observed for heavy biomolecules in Matrix-Assisted Laser Desorption Ionization (MALDI),[14] indicating that the observed ejecta were likely nanoparticles. Measurement of the FWHM of an actual deposit showed an angular spread of

a)Email: rouleaucm@ornl.gov. Tel.: 865-574-5499.

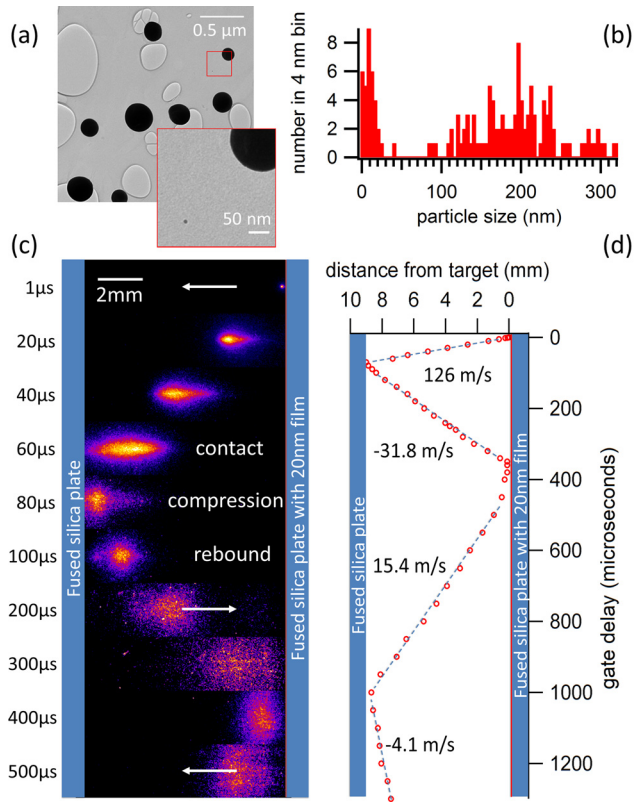

FIG. 1. Particle morphology (a), particle size distribution (b), false color ICCD image sequence at fixed gain and f-stop (c), and position of maximum plume intensity vs. time plot derived from time-resolved ICCD imaging of a 20 nm Pt film irradiated in vacuum at an incident fluence of 40–60 mJ/cm^2 (d). The gate width used for imaging was 20% of the respective gate delay, and particle collection was performed at a distance of 5 mm on a lacey carbon TEM grid. The size histogram was the result of 3600 ablation events from unique locations, and derived by measuring the diameter of ~200 particles in a series of TEM micrographs. The laser entered the source substrate at the right, and ejecta traveled to the left as a compact mm-scale packet having a collective velocity of 126 m/s as shown in the range vs. time plot. Three rebound events were observed thereafter, wherein the velocity was reduced with each bounce.

~2.6°,[13] which is in good agreement with the value of the included angle defined by the bright waist of the plume in the figure. Spectrally resolved imaging of the plume through a series of 40 nm optical bandpass filters revealed blackbody-like spectra at time delays of 5 μs and 50 μs after ablation, which, after radiometric calibration, permitted temperature estimates of ~1900 K and ~1700 K, respectively, consistent with incandescent Pt nanoparticles that were nearly molten.

To gain insight into the composition of the plume, a lacey carbon TEM grid was placed on the receiving substrate located 5–10 mm from the source substrate, and the captured material was analyzed by TEM. As shown in Fig. 1(a), the deposit was composed of large and small (see inset) spherical nanoparticles, and as shown in Fig. 1(b), their size distribution was bimodal with one mode centered near 10 nm and the other near 200 nm. Separate experiments to slow the ejecta with high background gas pressures indicated that the small mode could be eliminated in the deposit, but without any noticeable change to ICCD images of the plume as in Fig. 1(c), thereby indicating that the present images follow the propagation of the primarily larger 80–320 nm nanoparticles in the large mode. Detailed comparison of the size-dependent particle slowing will be the subject of a separate publication.[15] Thus, the physical origin and the time/place of the formation of the small nanoparticles are subject to interpretation. Three possible scenarios may be considered for the mechanisms of nanoparticles formation: (1) splashing or fragmentation of larger nanoparticles upon impact on the receiver, (2) condensation of ablated atomic species, or (3) generation at the early stage of the ablation of the film and simultaneous ejection with the large nanoparticles.

To evaluate the splashing contribution, the material transport from the source and its interaction with the receiver were analyzed by time-resolved imaging. The sequence of plume images in Fig. 1(c) not only revealed rebounding of the plume from the surface of the receiver, but from the source as well. A total of 3 rebound events were observed as shown in the distance versus time plot of Fig. 1(d). This points out that particle size distributions measured using witness plate techniques may be skewed with respect to the *true* distribution in the incoming plume. Note that while some of the nanoparticles rebounded from the receiving substrate (Figs. 1(c) and 1(d)) and others were collected and contributed to the large-size mode of the particle size distribution (Fig. 1(b)), it is reasonable to consider a question on whether fragmentation or splashing of the larger nanoparticles represent a possible alternative outcome of the nanoparticle interaction with the substrates.

An examination of the Reynolds, Weber, and Ohnesorge numbers for an impinging particle does provide some guidance as to whether fragmentation was likely. The Reynolds number, *Re,* for Pt particles with diameters <300 nm (Fig. 1(b)), mean velocity of 126 m/s (Fig. 1), and dynamic viscosity and density (at 1600 K) of 9.5 mPa s and 20.6 g/cc, respectively,[16] would have been *less than* 95. Similarly, with the above parameters and the surface tension of Pt at 1600 K taken as 1.72 N/m,[16] the Weber number, *We*, would have been *less than* 75. Lastly, the Ohnesorge number, $Oh=We^{1/2}/Re$, that relates viscous forces to the inertia and surface tension of the particle, would therefore have been *greater than* 0.1 under the present conditions.

To determine if splashing was likely, one needs to estimate a critical Ohnesorge number, Oh_{cr}. Using the formalism of Mundo *et al.*,[17] and references therein, Oh_{cr} can be shown to be not only a function of the contact angle of the particle at maximum spread, but the ratio of the maximum spread of the particle on impact to its original diameter. For high viscosity liquids, *Re* and *We* as above, and using the formalism by Mao *et al.*,[18] it can be shown that the latter ratio is ~2 for a wide range of contact angles. This leaves one to estimate a contact angle, and a reasonable assumption here is that it was greater than 90°, due to the relatively high viscosity of Pt particles under the present conditions. Consequently, Oh_{cr} was always *less than* 0.1, and since it marks the boundary *below* which splashing is considered likely, it can be concluded that splashing-induced nanoparticle generation was *not* likely under the present conditions.

Turning to gas-phase condensation as a possible source of the small mode in Fig. 1(b), this scenario was tested recently by comparing the size distribution of particles collected in vacuum to that of particles collected in 1 Torr Ar gas.[13] The same 10 nm source film and 5 mm distance to the receiving substrate were used in both cases, and both distributions were found to be bimodal with one mode near 10 nm and the other near 120 nm. Most notable was that in contrast

to ns-ablation of thin metal films,[12] *no* change in the magnitude of the smaller mode was observed upon performing the collection at 1 Torr. This observation is *inconsistent* with the hypothesis of condensation being the source of the small nanoparticles in the small mode.

We are left with the last possible interpretation that the small nanoparticles directly form in the film ablation process. To understand the highly nonequilibrium process the initial stage of fs laser ablation of a 20 nm Pt film is investigated here using an atomistic simulation performed with a hybrid TTM-MD model[19–21] that combines a classical molecular dynamics (MD) method with a continuum description of the laser excitation of conduction band electrons, electron-phonon coupling, and electron heat conduction based on a two-temperature model (TTM).[22] The dimensions of the computational system in the lateral (parallel to the surface of the film) directions were 100 nm × 100 nm and the total number of atoms in the system was 13.3×10^6. The interatomic interactions in the Pt film were described by the embedded atom method potential[23] and the parameters of the TTM equation for the electron temperature are from Ref. 24. The transparent silica substrate was represented by a dynamic acoustic impedance matching boundary condition that accounted for the elastic response of the substrate and reproduced the work of adhesion between Pt and fused silica.[25] A detailed description of the model used in the simulations of thin film ablation will be provided elsewhere.[26]

The conditions leading to the ejection and disintegration of the 20 nm Pt film irradiated by a 40 fs laser pulse at an absorbed fluence of 37 mJ/cm^2 (about 2.4 times the threshold fluence for complete melting of the film) are illustrated in Fig. 2. The excitation of electrons within the optical penetration depth followed by the rapid energy redistribution by the excited electrons results in the homogeneous heating of the film (Fig. 2(a)) on the timescale of the electron-phonon equilibration, $\tau_{e\text{-}ph} \approx 6$ ps, defined here as the time constant of the exponential decay of the energy of the excited electrons.

The fast heating occurring under conditions of stress confinement[19–21,27] ($\tau_{e\text{-}ph} \leq L_f/C_s \approx 7$ ps, where $L_f = 20$ nm is the thickness of the film and $C_s \approx 3000$ m/s is the speed of sound in Pt) leads to the buildup of high compressive pressure (Fig. 2(b)). In agreement with predictions of earlier atomistic[19] and continuum-level simulations,[28] the relaxation of the compressive pressure causes rapid expansion of the film and generation of strong tensile stresses in the upper portion of the film 8 to 15 ps after the laser pulse. The tensile stresses induce cavitation and eventual disintegration/spallation of the film into a thicker layer adjacent to the substrate and a thinner layer moving away from the substrate with a velocity of ~300 m/s. As shown in the inset of Fig. 2(d), the pressure from the vapor released in the process of the film disintegration and subsequent evaporation from the liquid fragments results in additional acceleration of the top layer, leading to a velocity of 480 m/s by the end of the simulation. The thicker layer also separates from the substrate and gradually accelerates to 110 m/s by 1.5 ns. The time dependences of the velocities of both layers show signs of saturation by 1.5 ns, and extrapolation to longer times suggests steady state values of ~500 m/s and ~150 m/s for the upper and lower parts of the film, respectively.

A visual picture of the film disintegration and ejection is provided in Fig. 3, where snapshots from the simulation are shown. The initial spallation of the film into two layers is

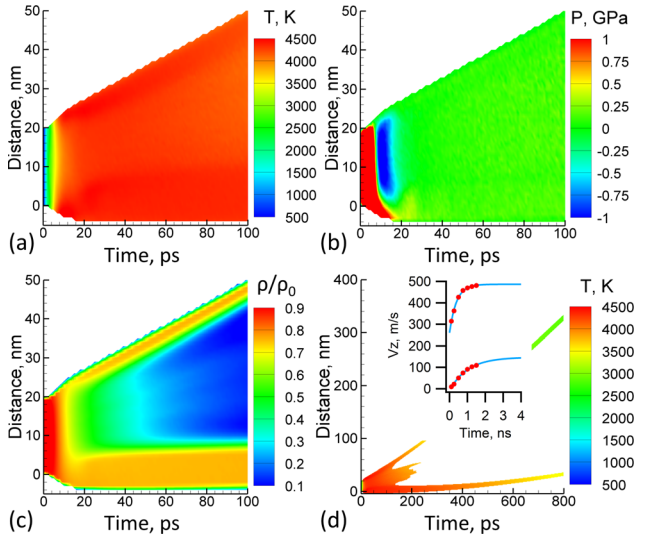

FIG. 2. Contour plots showing the evolution of temperature (a) and (d), pressure (b), and density (c) in a TTM-MD simulation of a 20 nm Pt film deposited on a silica glass substrate and irradiated by a 40 fs laser pulse at an absorbed fluence of 37 mJ/cm^2. The density scale is normalized to the initial density before the irradiation, ρ_0. Areas where the density of the material is less than $0.05\rho_0$ are not shown in the plots. The laser pulse is directed through the silica substrate, i.e., along the Y-axis from the bottom of the contour plots, and the distance on the Y-axis is from the initial position of the Pt/substrate interface. The inset in (d) shows the time dependence of the ejection velocity of the upper and lower portions of the film that is split during the ablation process.

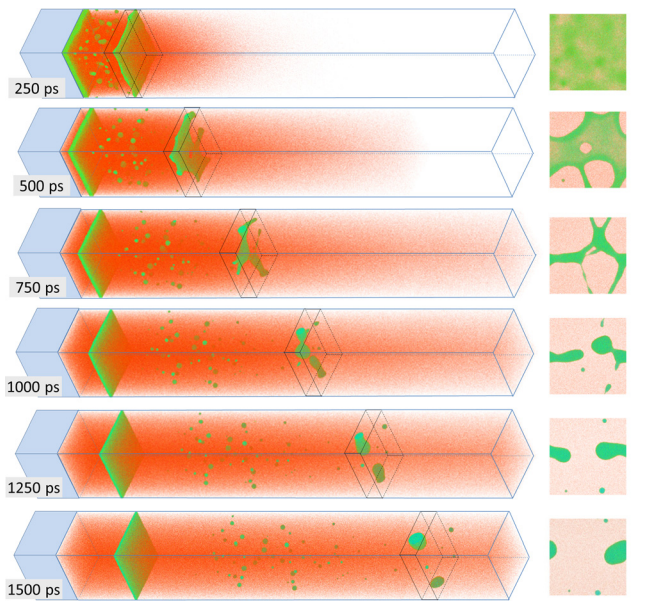

FIG. 3. Snapshots of atomic configurations predicted in a TTM-MD simulation of laser ablation of a 20 nm Pt film irradiated by a 40 fs laser pulse at an absorbed fluence of 37 mJ/cm^2. The atoms are colored by their potential energies, from red, for the vapor-phase atoms, to green, for atoms in liquid droplets. The square frames shown on the right are plan views of 30 nm sections of the plume outlined in the snapshots. Note that the laser pulse enters the film from the left, through the transparent substrate shown by the blue rectangular parallelepipeds.

followed by a rapid decomposition of the upper molten layer into a 28 nm diameter droplet with three smaller clusters (see 1.5 ns snapshot). While the small (100×100 nm^2) lateral size of the computational system does not allow us to predict the particle size distribution emerging from the layer decomposition, we can conclude that the particle diameters are in the range of tens of nm. Similarly, while the thicker lower spalled layer is stabilized by the periodic boundary conditions and retains its integrity during the simulation, the layer can be expected to decompose into individual droplets under conditions realized in the present experiments. Using a theoretical analysis of the stability of thin liquid films developed by Vrij[29] and applied to spalled layers in Ref. 21, droplets with diameters of ~160 nm are estimated from the dominating perturbation wavelength leading to spontaneous rupture of the film.[21]

Making connections to the experimental observations, the small mode of the bimodal distribution in Fig. 1(b) can be attributed to droplets in the range of tens of nm that originate from the fast moving portion of the film that spalls in the early stages of ablation, as well as the small clusters that form in the spallation process and are located between the fast and slower moving portions of the film (Fig. 3). On the other hand, the droplets contributing to the large mode of the size distribution in Fig. 1(b) are expected to result from the rupture of the slower moving portion of the film, as both the sizes of the larger droplets, in hundreds of nm, and the ejection velocity, ~150 m/s, are in a good agreement with the measured values. Moreover, the computational prediction that the large particles originate from decomposition of a liquid layer moving away from the irradiated target with a common collective velocity is consistent with the observation of the detached compact plumes in the ICCD images in Fig. 1(c).

While the initial temperature of the droplets in the simulations is ~4000 K, by 1.5 ns fast evaporative cooling brings the temperature of the top and bottom layer down to 2570 K and 2850 K, respectively. Additional evaporative cooling combined with radiative energy loss can be expected to bring the temperature below the melting point and cause solidification on a timescale of μs.[30] This scenario is consistent with the temperatures of ~1900 K and ~1700 K evaluated from spectrally resolved imaging of the plume at 5 and 50 μs, respectively.

Based on the insights into the origin of the bimodal size distribution provided by the simulations, the conditions for the transition from a bimodal to unimodal size distribution can be suggested. Since splitting of the film into two layers contributing to the two modes of the particle size distribution is defined by the conditions of stress confinement, a decrease in film thickness, L_f, would necessarily reduce the magnitude of the laser-induced compressive and tensile stresses, thereby preventing the film from splitting. To verify this prediction, nominally 15, 10, 5, and 2 nm films were ablated and the particle size distributions were analyzed. The results are shown in Fig. 4, and most notable is the collapse of the two modes of the distribution into a *single* mode as the nominal film thickness approaches 2 nm, thereby confirming the computational prediction.

In summary, the generation and transport dynamics of Pt nanoparticles synthesized by backside fs-laser ablation of optically thin Pt films on a transparent substrate was investigated experimentally and computationally. Multiple rebound events were observed in particle collection experiments, suggesting that the size distributions measured using witness plates may represent skewed versions of the nascent distributions generated in fs-ablation. In nearly all cases, the collected distributions were bimodal, with one mode in the tens of nm range, and the other in the hundreds of nm range. The results of a TTM-MD simulation suggest that the smaller mode largely originated from a thin, fast-moving layer that spalled in the early stage of ablation, leaving an underlying, slower-moving unstable liquid layer wholly responsible for the larger mode. Generation of smaller particles by gas phase condensation in the ablation plume or through splashing of the larger particles upon impact was ruled unlikely under the present conditions. Finally, in agreement with modeling, the reduction in film thickness from 20 to 2 nm was found to result in a commensurate shift in the large mode of the particle size distribution toward smaller mean values until finally, at a nominal thickness of 2 nm, the distribution became unimodal. These results suggest a synthesis route for production of nanoparticles with a narrow size distribution in the range of tens of nm, delivered to a surface in a localized and well-controlled fashion.

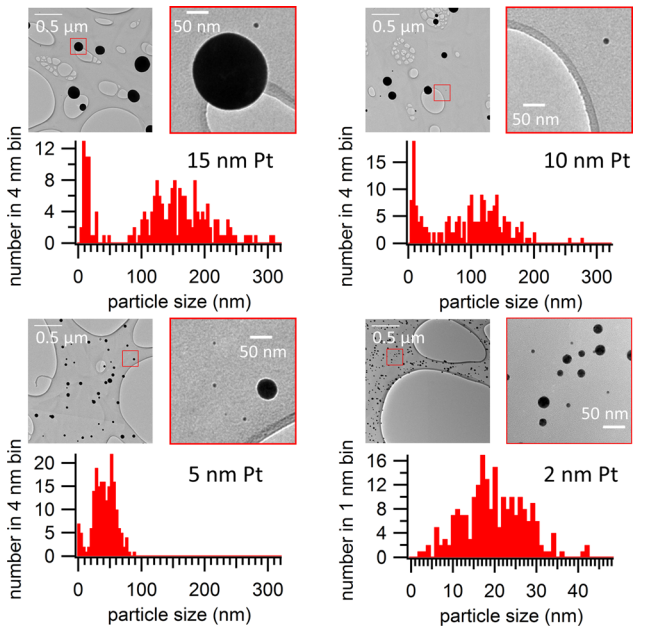

FIG. 4. Particle size distribution and representative TEM images at high and low magnifications as a function of nominal film thickness (shown). In all cases, particle collection was performed in vacuum, at 5 mm, and using an incident fluence of 40–60 mJ/cm^2.

Research was sponsored by the Materials Sciences and Engineering Division, Office of Basic Energy Sciences, U.S. Department of Energy (synthesis science). A portion of this research was conducted as a user project at the Center for Nanophase Materials Sciences user facility, which is sponsored at Oak Ridge National Laboratory by the Scientific User Facilities Division, U.S. Department of Energy. Computational studies were funded by the National Science Foundation through Grants DMR-0907247 and CMMI-1301298, and the Air Force Office of Scientific Research

through Grant FA9550-10-1-0541. Computational support was provided by NSF through the Extreme Science and Engineering Discovery Environment (Project TG-DMR110090) and by the Oak Ridge Leadership Computing Facility (Project MAT048).

[1]*Metal Nanoparticles and Nanoalloys*, edited by R. L. Johnston and J. P. Wilcoxon, Frontiers of Nanoscience Series Vol. 3, edited by R. E. Palmer (Elsevier, Amsterdam, 2012), p. 312.
[2]N. G. Semaltianos, Crit. Rev. Solid State **35**, 105–124 (2010).
[3]S. Barcikowski and G. Compagnini, Phys. Chem. Chem. Phys. **15**, 3022–3026 (2013).
[4]M. E. Povarnitsyn, T. E. Itina, M. Sentis, K. V. Khishchenko, and P. R. Levashov, Phys. Rev. B **75**, 235414 (2007).
[5]S. Amoruso, R. Bruzzese, X. Wang, N. N. Nedialkov, and P. A. Atanasov, J. Phys. D: Appl. Phys. **40**, 331 (2007).
[6]S. Amoruso, R. Bruzzese, X. Wang, and J. Xia, Appl. Phys. Lett. **92**, 041503 (2008).
[7]S. Noël and J. Hermann, Appl. Phys. Lett. **94**, 053120, 2009.
[8]K. Oguri, Y. Okano, T. Nishikawa, and H. Nakano, Phys. Rev. B **79**, 144106 (2009).
[9]N. Haustrup and G. M. O'Connor, Appl. Phys. Lett. **101**, 263107 (2012).
[10]T. Donnelly, J. G. Lunney, S. Amoruso, R. Bruzzese, X. Wang, and X. Ni, J. Appl. Phys. **108**, 043309 (2010).
[11]R. Murphy, B. Torralva, and S. Yalisove, Appl. Phys. Lett. **102**, 181602 (2013).
[12]P. T. Murray and E. Shin, "Synthesis of Ag nanoparticles by through thin film ablation," in *Silver Nanoparticles*, edited by D. P. Perez (InTech, 2010), pp. 145–152.
[13]C. M. Rouleau, M. Tian, A. A. Puretzky, M. Mahjouri-Samani, G. Duscher, and D. B. Geohegan, Proc. SPIE **8969**, 896907 (2014).
[14]A. A. Puretzky, D. B. Geohegan, G. B. Hurst, M. V. Buchanan, and B. S. Luk'yanchuk, Phys. Rev. Lett. **83**, 444 (1999).
[15]C. M. Rouleau, A. A. Puretzky, and D. B. Geohegan, "Transport dynamics of nanoparticles generated by femtosecond laser ablation of thin metal films in a background gas" (unpublished).
[16]T. Ishikawa, P. F. Paradis, J. T. Okada, and Y. Watanabe, Meas. Sci. Technol. **23**, 025305 (2012).
[17]C. Mundo, M. Sommerfeld, and C. Tropea, Int. J. Multiphase Flow **21**, 151–173 (1995).
[18]T. Mao, D. C. S. Kuhn, and H. Tran, AIChE J. **43**, 2169–2179 (1997).
[19]D. S. Ivanov and L. V. Zhigilei, Phys. Rev. B **68**, 064114 (2003).
[20]L. V. Zhigilei, Z. Lin, and D. S. Ivanov, J. Phys. Chem. C **113**, 11892–11906 (2009).
[21]C. Wu and L. V. Zhigilei, Appl. Phys. A **114**, 11–32 (2014).
[22]S. I. Anisimov, B. L. Kapeliovich, and T. L. Perel'man, Sov. Phys. JETP **39**, 375–377 (1974).
[23]S. M. Foiles, M. I. Baskes, and M. S. Daw, Phys. Rev. B **33**, 7983–7991 (1986).
[24]Z. Lin, L. V. Zhigilei, and V. Celli, Phys. Rev. B **77**, 075133 (2008).
[25]R. Yu, H. Song, X. F. Zhang, and P. D. Yang, J. Phys. Chem. B **109**, 6940–6943 (2005).
[26]C.-Y. Shih, C. Wu, M. Shugaev, C. M. Rouleau, A. A. Puretzky, D. B. Geohegan, and L. V. Zhigilei, "Mechanisms of nanoparticle generation in femtosecond laser ablation of thin metal films" (unpublished).
[27]L. V. Zhigilei and B. J. Garrison, J. Appl. Phys. **88**, 1281–1298 (2000).
[28]M. V. Shugaev and N. M. Bulgakova, Appl. Phys. A **101**, 103–109 (2010).
[29]A. Vrij, Discuss. Faraday Soc. **42**, 23–33 (1966).
[30]L. Landström and P. Heszler, J. Phys. Chem. B **108**, 6216–6221 (2004).